Journal of Materials Chemistry B

Accepted Manuscript

ROYAL SOCIETY OF CHEMISTRY

www.rsc.org/materialsB

Journal Name

RSCPublishing

ARTICLE

Ho^{3+} doped $NaGdF_4$ nanoparticles as MRI/optical probes for brain glioma imaging

Cite this: DOI: 10.1039/x0xx00000x

Received 00th January 2012,
Accepted 00th January 2012

DOI: 10.1039/x0xx00000x

www.rsc.org/

Yunlong Deng,[a,#] Hao Wang,[b,#] Wei Gu,[a] Shuai Li,[a] Ning Xiao,[a] Chen Shao,[a] Qunyuan Xu[b,*] and Ling Ye[a,*]

Lanthanide-ion doped $NaGdF_4$ nanoparticles (NPs) have been exploited as a new generation of MRI/optical probes. However, it remains difficult for these NPs to image tiny brain gliomas due to low specificity and limited accumulation. To circumvent this obstacle, chlorotoxin (CTX) was conjugated onto Ho^{3+} doped $NaGdF_4$ (CTX-$NaGdF_4$:Ho^{3+}) to render a glioma-specific targeted MRI/optical probe. Both confocal laser scanning microscopy and flow cytometry demonstrated the targeting ability of CTX-$NaGdF_4$:Ho^{3+} NPs towards glioma cells *in vitro*. Furthermore, *in vivo* MRI and fluorescence imaging of the tiny brain gliomas in mice confirmed that the CTX-$NaGdF_4$:Ho^{3+} NPs could lead to a significant contrast enhancement effect and a clearer boundary between glioma and normal tissue. In addition, the CTX-$NaGdF_4$:Ho^{3+} NPs exhibited a low cytotoxicity and no detectable tissue damages. Therefore, the CTX-$NaGdF_4$:Ho^{3+} NPs could potentially serve as an MRI/optical probe for the detection of tiny brain gliomas.

Introduction

Gliomas are the most common and aggressive primary brain malignancies. The detection of brain glioma at its earliest stage is crucial to decrease the mortality and disability rate.[1-4] Magnetic resonance imaging (MRI) has been widely recognized as an effective non-invasive diagnostic tool to identify the macroscopic outline of glioma and guide the stereotactic surgery.[5-7] The use of contrast agents (CAs) helps enhance the contrast effect between glioma and normal tissue. However, clinically approved low molecular weight gadolinium (Gd) chelates such as Gd-DTPA and Gd-DOTA[8, 9] are limited in detecting brain tumors because they suffer from a rapid renal clearance, which results in an insufficient concentration in the tumor site and thus shows a relatively low contrast effect.

Gd-containing nanoparticles (NPs) are alternative efficient CAs due to a long blood retention time, easy surface conjugation and low toxicity.[10, 11] Recently, $NaGdF_4$ NPs have been exploited as a new generation of MRI contrast agents.[12, 13] For example, Gao et al.[14] prepared $NaGdF_4$ NPs with r_1 of 5.7 mM^{-1} s^{-1} and confirmed that those $NaGdF_4$ NPs significantly enhanced the contrast effect in the intraperitoneal xenograft glioma. In addition to serving as MRI probes, lanthanide-ion doped $NaGdF_4$ NPs have been reported as optical nanoprobes in down- and/or up-conversion manner. The lanthanide-ion doped $NaGdF_4$ NPs thus provide the dual modality of optical and MR imaging. As can be imaged in different ways to provide complementary information, they are undoubted beneficial in improving the diagnosis efficacy of early brain glioma and subsequent optical guidance for surgery. Lee et al.[15] synthesized core–shell $NaYF_4$:Yb,Er/$NaGdF_4$ NPs and those NPs exhibited green/red luminescence as well as MRI enhancement in the xenograft U87MG tumor. However, the application of lanthanide-ion doped $NaGdF_4$ NPs in brain glioma MRI is still limited by low target specificity.

An active targeting strategy to improve the specificity and cellular uptake is through the attachment of targeting moieties. Although various target molecules such as folic acid,[16] Tat peptide[17] and transferrin[18] have been used as targeting moieties, chlorotoxin (CTX), a 36-amino acid peptide from scorpion venom,[19] has been proved to be the most efficient targeting moiety for the vast majority of brain tumors.[20-22] Zhang's group[23] confirmed that CTX conjugation substantially enhanced the uptake of iron oxide NPs by brain tumor cells and led to an enhanced MR

[a] *School of Chemical Biology and Pharmaceutical Sciences, Capital Medical University, Beijing, 100069, P. R. China.*
[b] *Regeneration and Repair, Key Laboratory for Neurodegenerative Disease of The Ministry of Education ,Capital Medical University, Beijing, 100069, P. R. China*
[#] *These authors contributed equally to this work.*
* *Corresponding authors. E-mail: lingye@ccmu.edu.cn; xuqy@ccmu.edu.cn; Tel: +86 10 83911525; Fax: +86 10 83911533.*

contrast. Therefore, we conjectured that the CTX-conjugated lanthanide-ion doped $NaGdF_4$ NPs should have high sensitivity and specificity toward gliomas. However, CTX-conjugated lanthanide-ion doped $NaGdF_4$ NPs as MRI/optical probes for the detection of tiny brain gliomas remains unexplored so far.

In addition, the colloidal stability is an important prerequisite to govern the blood circulation behaviour of the NPs. Usually, $NaGdF_4$ NPs are synthesized by the thermal decomposition of metal precursors in organic medium to ensure the uniform size and high crystallinity. The OA-capped hydrophobic $NaGdF_4$ NPs are then transformed to hydrophilic ones by ligand-exchange. Although oleic acid (OA) ligands of $NaGdF_4$ particles were successfully exchanged with polyethylenimine (PEI),[24] 3-mercaptopropionic acid (MPA)[25] and citrate,[26] these exchanged ligands were noncovalently bound to the NPs, which might affect the long-term stability. Therefore, a covalently linked ligand is highly desirable in the term of stability.

Herein, the OA-capped, Ho^{3+} doped $NaGdF_4$ NPs were first prepared by thermal decomposition method. The OA ligands were then replaced by carboxylic silane. The covalently linked silane not only endows highly water-dispersible and stability, but also provides abundant carboxylic groups for conjugation of CTX ligands to yield CTX-conjugated Ho^{3+} doped $NaGdF_4$ (CTX-$NaGdF_4$:Ho^{3+}) NPs as a potential glioma-specific MRI/optical nanoprobe. The targeting ability of the CTX-$NaGdF_4$:Ho^{3+} NPs toward C6 glioma cells was evaluated by confocal laser scanning microscopy (CLSM) and flow cytometry. The contrast enhancement between glioma and normal tissue was further investigated in tiny brain glioma-bearing mice. Additionally, the toxicity of CTX-$NaGdF_4$:Ho^{3+} NPs was evaluated by MTT assays and hematoxylin and eosin (H&E) staining.

Experimental

Materials

1-octadecene (ODE, > 90%) and oleic acid (OA, > 90%) were purchased from Sigma–Aldrich (USA). Gadolinium (III) oxide (Gd_2O_3, 99.99%), Holmium (III) oxide (Ho_2O_3, 99.99%), sodium fluoride (NaF) were obtained from Sinopharm Chemical Reagent Co. Ltd. (Beijing, China). *N*-(trimethoxysilypropyl) ethylene diamine triacetic acid, trisodium salt (TETT) (45% in water) was supplied by Gelest Inc. (USA). Chlorotoxin (CTX) was purchased from Gl Biochem Ltd (Shanghai, China). N-Hydroxysuccinimide (NHS) was acquired from Acros Oganics (Geel, Belgium). N-(3-Dimethylaminopropyl-N'-ethylcarbodiimide hydrochloride (EDC) was provided by J&K Chemical Ltd. (Shanghai, China). Fetal bovine serum (FBS) and Dulbecco's modified eagle's medium (DMEM) were supplied by Gibco (Basel, Switzerland).3-(4,5-dimethylthiazolyl-2)-2,5-diphenyltetrazolium bromide (MTT) cell proliferation assay kit was received from Amresco (Solon, USA).

Synthesis of OA-capped $NaGdF_4$:Ho^{3+} (OA-$NaGdF_4$:Ho^{3+}) NPs

OA-capped $NaGdF_4$:Ho^{3+} NPs were synthesized by a one-pot synthetic approach. Briefly, 1.3436 g of NaF and 2 mmol of $Ln(oleate)_3$ (Gd^{3+}:Ho^{3+} = 0.95:0.05, mole-to-mole ratio) were added to 20 mL of ODE containing 5 mL of OA. After degassing under vacuum for 1 h, the mixture was heated rapidly to 290 ºC and maintained at this temperature for 90 min with vigorous mechanical stirring under a nitrogen flow. Then, the reaction mixture was cooled to room temperature naturally Subsequently, absolute ethanol (20 mL) was added and the precipitates were separated by centrifugation, washed with ethanol three times to remove the excess ODE and OA. The obtained OA-$NaGdF_4$:Ho^{3+} NPs were redispersed in hexane for further use.

Synthesis of TETT silane modified $NaGdF_4$:Ho^{3+} (TETT-$NaGdF_4$:Ho^{3+}) NPs

The TETT-$NaGdF_4$:Ho^{3+} NPs were prepared by a ligand exchange method.[27] In brief, 100 mg of OA-capped $NaGdF_4$:Ho^{3+} NPs were dispersed in 50 mL of toluene, followed by addition of 60 μL of acetic acid. After sonicating for 15 min, 1.2 mL of TETT silane was added and the mixture was stirred at 70 ºC for 48 h. The precipitated TETT-$NaGdF_4$ Ho^{3+} NPs were collected and purified by washing with toluene and methanol sequentially. The product was resuspended in water and dialyzed against deionized water for 24 h using a cellulose dialysis bag (MWCO = 3,500 Da). The purified aqueous sample was lyophilized to yield the TETT-$NaGdF_4$:Ho^{3+} powder.

Synthesis of CTX-conjugated $NaGdF_4$:Ho^{3+} (CTX-$NaGdF_4$:Ho^{3+}) NPs

100 mg of TETT-$NaGdF_4$:Ho^{3+} NPs was dispersed in 20 mL of PBS (0.1 M, pH = 6.0), followed by the addition of 47 μg of NHS and 70 μg of EDC. The mixture was then allowed to react with 3 mg of CTX at room temperature for 48 h in PBS at pH 8. When the reaction was completed, the suspension was dialyzed against deionized water for 24 h using a cellulose dialysis bag (MWCO = 14,000 Da) and then lyophilized to obtain CTX-$NaGdF_4$:Ho^{3+} NPs.

Characterization

X-ray diffraction (XRD) was carried out with a Rigaku SmartLab X-ray diffractometer (Cu K_α radiation λ=1.54056 Å) operating at 45 kV and 200 mA. Transmission electron microscopy (TEM) images were obtained on a JEM-2100F (JEOL, Japan) at operating voltage of 120 kV. Dynamic light scattering (DLS) and zeta potential measurements were performed on a Nano-ZS90 Zetasizer (Malvern, UK). Fourier transform infrared (FTIR) spectra of NPs were collected on a Nicolet Avatar 300 FT-IR spectrometer (Thermo Nicolet

Instrument Corp., USA). As-prepared NPs were mixed with KBr and then pressed into a pellet with the minimum pressure. A total of 100 scans were accumulated with a resolution of 4 cm^{-1} for each spectrum. Inductively coupled plasma-atomic emission spectrometry (ICP-AES) analysis was conducted on a Thermo X-Series II (X7) quadruple ICP-AES (SPECTRO Analytical Instruments GmbH., Germany). Fluorescence emission spectrum was recorded on an F-2500 fluorescence spectrophotometer (Hitachi, Japan).

Cell culture and animal model

C6 glioma cells and NIH 3T3 cells were cultured in Dulbecco's modified Eagle's medium (DMEM) supplemented with 10% fetal bovine serum (FBS), streptomycin (100 μg/mL) and penicillin (100 U/mL) at 37 °C in a humidified 5% CO_2 atmosphere. Nude mice bearing C6 glioma was prepared according to a reported protocol.[28] Briefly, 5×10^5 C6 glioma cells, suspended in 5 μL phosphate buffer solution (PBS), were injected into the left striatum (2 mm lateral to the bregma at 4 mm depth) of 4-6 weeks old male BALB/c nude mice with a chromatography syringe using a stereotactic fixation device equipped with a mouse adapter. All animal experiments were performed according to protocols evaluated and approved by the ethical committee of Capital Medical University (Beijing, China).

***In vitro* cytotoxicity assay**

The cytotoxicity of TETT-$NaGdF_4$:Ho^{3+} and CTX-$NaGdF_4$:Ho^{3+} NPs was evaluated via MTT colorimetric assay. C6 glioma and NIH 3T3 cells were seeded in a 96-well plate at a density of 1×10^5 cells per well. After 24 h of incubation, the medium was replaced by the suspension containing NPs at different concentrations and subsequently incubated for 4 or 24 h. Then, MTT (100 μL, 0.5 mg/mL) was added to each well and the plate was incubated for another 4 h. The growth medium was removed and DMSO (150 μL) was then added to each well. Finally, the absorbance at 570 nm was measured using a Multiskan Spectrum microplate reader (Thermo Electron Corp., USA). The cell viability was assessed by the ratio of OD values between experimental group and control group. Data were presented as the mean value with standard deviations from three independent experiments.

Histology

The ICR mice were sacrificed 15 days after injection of TETT-$NaGdF_4$:Ho^{3+} NPs or CTX-$NaGdF_4$:Ho^{3+} NPs at a dosage 500 μg Gd/kg. The major organs (heart, liver, kidney, spleen, lung and brain) were collected and fixed in freshly prepared formalin 10% for 72 h. Then, the tissues were dehydrated using a Tissue Processor, embedded with paraffin, snap-frozen, cryosectioned into 5 μm slices, and stained with hematoxylin and eosin (H&E) for 10 min according to standard clinical pathology protocols. The histological sections were observed on an optical microscope.

Confocal imaging of cells

C6 cells (1×10^5/well) were incubated with NPs (2.5 μg Gd/mL) in the confocal dish for 12 h at 37 ºC under 5% CO_2. After washing with PBS for three times, the nuclei were stained with 2 μg/mL 40-6-Diamidino-2-phenylindole (DAPI) for 10 min. The confocal dish was mounted and examined on a LEICA TCS SP5 confocal microscope (Leica Microsystems, Germany) using a 60 × oil-immersion objective lens with excitation at 405 and 458 nm for DAPI and NPs, respectively.

Flow cytometry

For the flow cytometry assay, C6 cells were seeded at a density of 1×10^5 cells per well in 24-well plates. Fresh medium containing TETT-$NaGdF_4$:Ho^{3+} or CTX-$NaGdF_4$:Ho^{3+} NPs (the equivalent Gd concentrations were set to be 0.625, 1.25, 2.5 and 5 μg/mL, respectively) was added and incubated with cells for 12 h. Then, the cells were washed with PBS and harvested by trypsinization. After centrifugation, the cell pellets were washed carefully with PBS, resuspended in PBS, and analyzed on a Guava EasyCyte Mini flow cytometry system (Millipore, USA).

Relaxivity measurement

T_1 relaxation times and corresponding R_1 maps of NPs at various Gd concentrations were acquired on a 7 T MRI instrument (Bruker) equipped with the knee coil (EXTREM). The NPs were dispersed in 1% agarose with a Gd concentration range from 0 to 0.6 mM. Relaxation rates ($1/T_1$) were measured and plotted against the concentration of Gd. The relaxivity of r_1 was then obtained from the slope of linear fitting. The T_1-weighted images were collected with the sequence of RARE-T_1+T_2-map (TR=1500ms and TE = 11 ms, 33 ms, 55 ms, 77 ms, 99 ms, matrix size = 256 × 256, field of view (FOV) = 4.0 × 4.0 cm^2, flip angle (FA) = 180° and slice thickness = 1 mm).

***In vivo* MRI**

The intracranial C6 glioma-bearing mice were anesthetized and scanned before and after the administration of as-prepared nanoparticles fourteen days after implantation. MRI was conducted on a 7T MRI scanner (Bruker Pharmascan, Germany) using a T_1-mapping sequence (TR = 400 ms, TE = 9.0 ms, Flip angle = 180°, matrix = 256 × 256, FOV = 3.0 × 3.0 cm^2, slice thickness = 0.8 mm). The PBS solution (150 µL) of the 250 μg Gd/kg nanoparticles (TETT-NaGdF4:Ho^{3+} NPs and CTX-NaGdF4:Ho^{3+} NPs) was injected intravenously and MRI coronal images were obtained for each animal.

Confocal imaging of brain slices

Balb/c mice bearing C6 glioma were injected by tail vein with TETT-$NaGdF_4$:Ho^{3+} or CTX-$NaGdF_4$:Ho^{3+} NPs at an equivalent concentration of 250 μg Gd/kg. One hour after injection, the mice were anesthetized and fixed by heart perfusion with saline and 4% paraformaldehyde. The brains were removed, fixed in 4% paraformaldehyde for 48 h, dehydrated sequentially with 30% sucrose solution for 24 h and 30% sucrose solution for 24 h until subsidence. Afterward, the brains were embedded in OCT (Sakura, Torrance, CA, USA) and frozen at -80 ºC, sectioned at 20 μm. After counterstaining with DAPI (100 ng/ml) for 10 min and triple rinsing with PBS, slides were visualized on a LEICA TCS SP5 confocal microscope using a 40 × dry objective lens.

Biodistribution

The glioma-bearing mice were randomly divided into two groups, which were treated with TETT-$NaGdF_4$:Ho^{3+} and CTX-$NaGdF_4$:Ho^{3+} NPs respectively. The glioma model mice were sacrificed 1 h after the injection of NPs via tail vein at a dose of 250 μg Gd/kg. The heart, liver, kidney, spleen, lung and brain were collected and the Gd content in each organ was determined by ICP-AES.

Statistical analysis

Data are presented as the mean ± SD. Statistical differences were evaluated using the Student's t test and considered significant at the $p < 0.05$ level.

Results and discussion

To ensure the high crystalline and size uniformity, OA-coated $NaGdF_4$:Ho^{3+} (OA-$NaGdF_4$:Ho^{3+}) NPs were synthesized by the thermal decomposition method and the crystalline structures of the NPs were determined by XRD analysis.

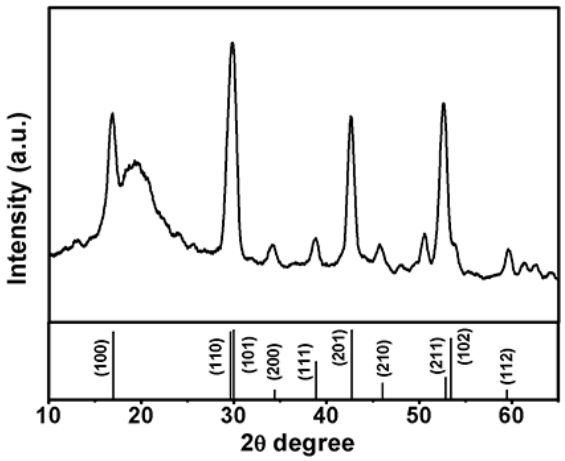

Fig. 1. XRD pattern of OA-$NaGdF_4$:Ho^{3+} NPs and JCPDS card No. 27-0699.

As shown in Fig. 1, the XRD pattern of OA-$NaGdF_4$:Ho^{3+} NPs showed characteristic diffraction peaks at 16.8°, 29.7°, 42.5°, and 52.6°, which can be indexed to (100), (110), (101), (201), and (211) reflections, respectively. The peak position and relative intensity matches the pattern for the hexagonal phase $NaGdF_4$ crystals (β-$NaGdF_4$) as reported in the JCPDS standard card (27-0699), implying a high crystalline quality of $NaGdF_4$:Ho^{3+} NPs regardless of Ho^{3+} doping. The additional broad peak at 20° confirmed the presence of OA ligands.

In order to obtain hydrophilic $NaGdF_4$:Ho^{3+} NPs, a ligand exchange reaction was performed by replacing OA ligands with carboxylic silane (TETT). The ligand exchange not only confers $NaGdF_4$:Ho^{3+} NPs highly water dispersible but also provides the carboxylic functional groups for the conjugation of target moiety CTX. Fig. 2 presents TEM images and DLS distribution profiles of OA-$NaGdF_4$:Ho^{3+}, TETT-$NaGdF_4$:Ho^{3+} and CTX-$NaGdF_4$:Ho^{3+} NPs, respectively. It was found that OA-$NaGdF_4$:Ho^{3+} NPs were short rod-shaped with approximately 18 nm in diameter (Fig. 2A). After ligand exchange with TETT, small clusters were found (Fig. 2B) and

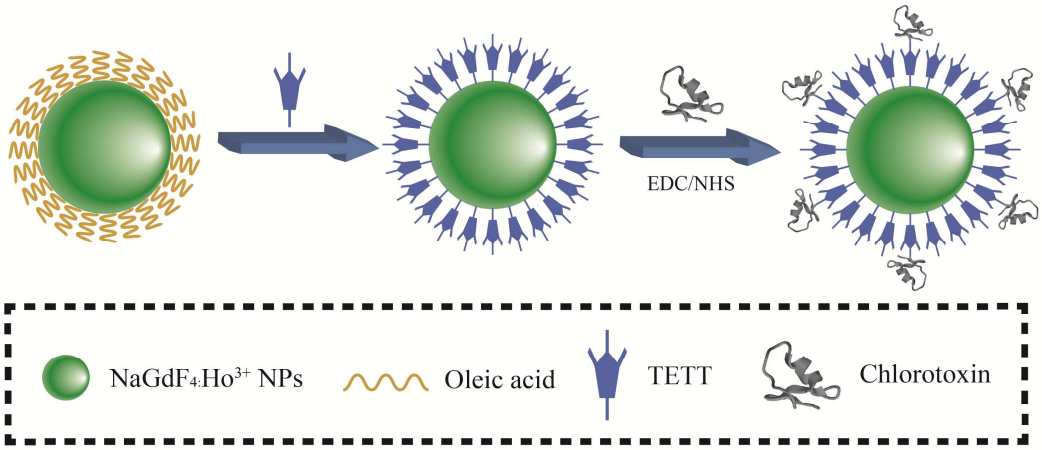

Scheme 1. Illustration of the synthesis of TETT-$NaGdF_4$:Ho^{3+} and CTX-$NaGdF_4$:Ho^{3+} NPs.

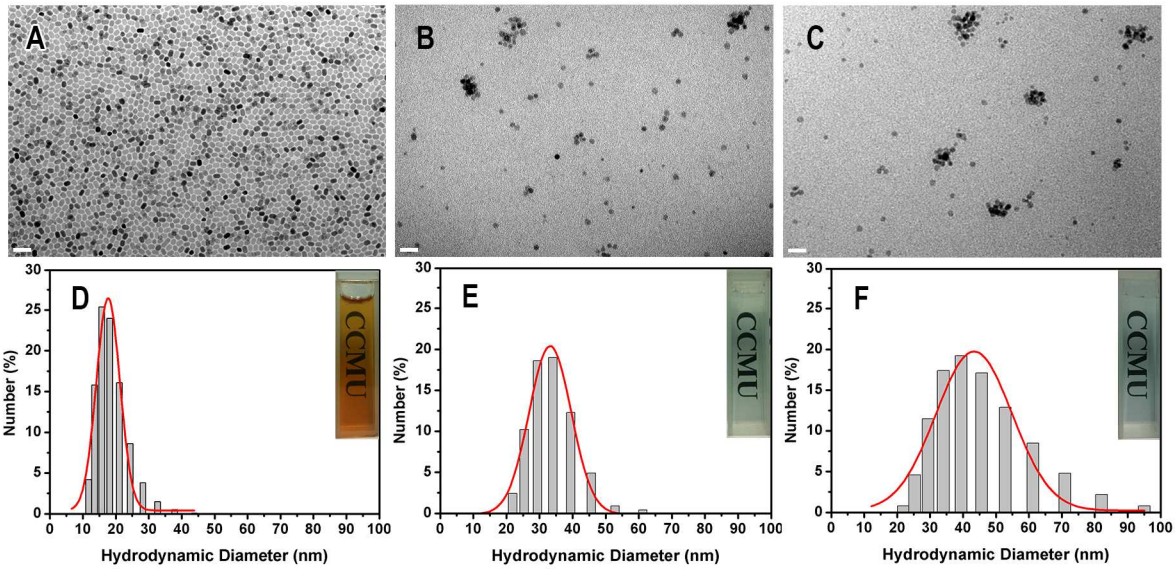

Fig. 2. TEM images of (A) OA- $NaGdF_4:Ho^{3+}$, (B) TETT-$NaGdF_4:Ho^{3+}$, (C) CTX- $NaGdF_4:Ho^{3+}$ NPs. Scale bar = 50 nm. Size distributions of (D) OA- $NaGdF_4:Ho^{3+}$, (E) TETT-$NaGdF_4:Ho^{3+}$ and (F) CTX- $NaGdF_4:Ho^{3+}$ NPs measured by DLS.

further conjugation of CTX to TETT-$NaGdF_4:Ho^{3+}$ NPs led to an increase in clustering (Fig. 2C). The corresponding dynamic light scattering (DLS) analysis showed the average size for OA-$NaGdF_4:Ho^{3+}$ NPs were 19.5 nm (Fig. 2D) in hexane, while the DLS value increased to 34.3 nm for TETT-$NaGdF_4:Ho^{3+}$ NPs (Fig. 2E) and 44.2 nm for CTX-$NaGdF_4:Ho^{3+}$ NPs (Fig. 2F). Although the increase in DLS, the two NPs still exhibit high stability at concentration of 30 mg/mL (see insets). Moreover, the size between 10 ~ 100 nm indicated these NPs would neither be easily taken up by macrophage cells of the reticulo-endothelial system (RES) nor be filtered out by the kidneys, making it favorable for the uptake by tumors.

The ligand exchange of OA with TETT and sequentially CTX conjugation was confirmed by Fourier transform infrared spectroscopy (Fig. 3A). For OA-$NaGdF_4:Ho^{3+}$ NPs, a pair of strong peaks at 2928 and 2858 cm^{-1} was attributed to the asymmetric and symmetric stretching vibration of the C-H bond of OA and another pair of peaks at 1565 and 1460 cm^{-1} was assigned to asymmetric and symmetric stretching vibration of carboxylic groups of bound OA ligands (Fig. 3a), respectively.[29, 30] Upon exchange of OA ligands with TETT silane, the OA characteristic bands disappeared and this was accompanied by the appearance of -COOH band at 1631 cm^{-1}, Si-O-Si band at 1128 cm^{-1}, and N–C band at 919 cm^{-1} [31](Fig. 3b), confirming the removal of oleic acid and the presence of TETT silane on the surface of NPs. The following conjugation of CTX to TETT-$NaGdF_4:Ho^{3+}$ NPs was verified by a slight blue shift of -COO^- band from 1631to 1624 cm^{-1} (Fig 3c) due to formation of amide bond.

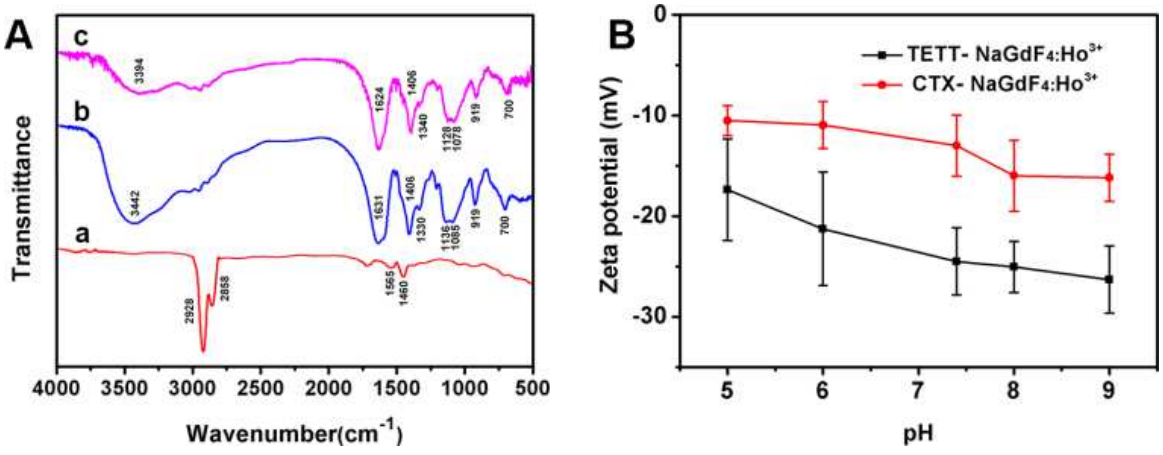

Fig. 3. (A) FTIR spectra of (a) OA-$NaGdF_4:Ho^{3+}$ NPs, (b) TETT-$NaGdF_4:Ho^{3+}$ NPs, (c) CTX-$NaGdF_4:Ho^{3+}$ NPs. (B) Zeta potential results of TETT-$NaGdF_4:Ho^{3+}$ NPs and CTX-$NaGdF_4:Ho^{3+}$ NPs. Each value was presented as the mean value ±S.D. of three runs.

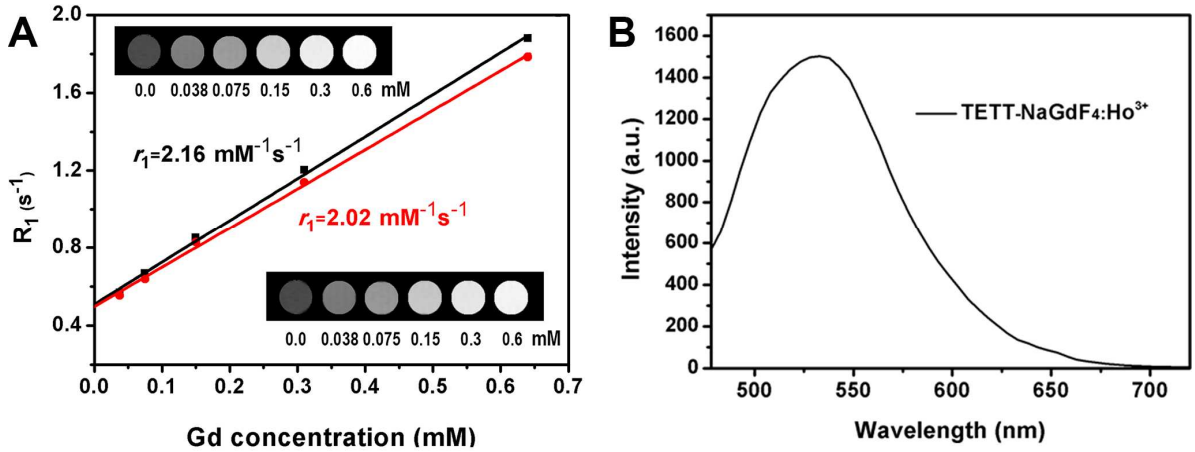

Fig. 4. (A) T_1-weight MR images of TETT-NaGdF$_4$:Ho^{3+} NPs at various Gd concentrations (0, 0.038, 0.075, 0.15, 0.3, 0.6 mM) and plotting of relaxation rate R_1 ($1/T_1$) versus Gd concentration. (B) Emission spectrum of TETT-NaGdF$_4$:Ho^{3+} NPs dispersed in PBS (λex = 458 nm).

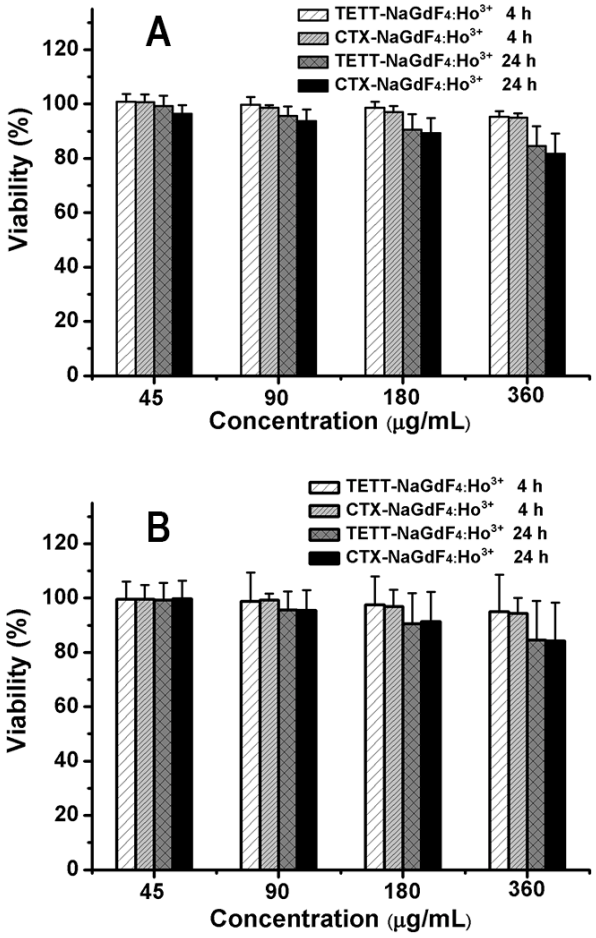

Fig. 5. Viability of C6 (A) and NIH 3T3 (B) cells 4 h and 24 h after incubation of TETT-NaGdF$_4$:Ho^{3+} or CTX-NaGdF$_4$:Ho^{3+} NPs with equivalent NPs concentrations (45, 90, 180, 369 μg/mL). Each result represents the mean ±S.D. of three experiments.

Additional evidence for the CTX conjugation was provided by the zeta potential measurements (Fig. 3B). At pH 5-9, TETT-NaGdF$_4$:Ho^{3+} NPs showed negative zeta potentials due to the deprotonation of carboxylic groups. The conjugation of CTX dramatically increased the zeta potential as a result of the consumption of carboxyl groups. The distinct difference in the overall zeta potentials between TETT-NaGdF$_4$:Ho^{3+} and CTX-NaGdF$_4$:Ho^{3+} NPs thus further supports the successful immobilization of CTX onto TETT-NaGdF$_4$:Ho^{3+} NPs.

To explore their potential as MRI/optical probes, the relaxivity performance and luminescent property of Ho^{3+} doped NaGdF$_4$ NPs were evaluated. The obtained R_1 maps of TETT-NaGdF$_4$:Ho^{3+} NPs on a 7T MRI scanner and corresponding r_1 relaxivity are illustrated in Fig. 4A. It was evidenced that as Gd concentration increased (from left to right), the R_1 maps showed a gradual increase in brightness (a higher concentration of Gd produced a brighter signal) and the longitudinal relaxivity (r_1) of TETT-NaGdF$_4$:Ho^{3+} and CTX-NaGdF$_4$:Ho^{3+} NPs was calculated to be 2.16 and 2.02 mM^{-1} s^{-1} respectively by plotting the relaxation rate ($1/T_1$) against the concentration of Gd. Although CTX conjugation led to a higher degree of cluster as observed on TEM image, such clustering played a minor effect on relaxivity in this case. Meanwhile, the emission spectrum of TETT-NaGdF$_4$:Ho^{3+} NPs in PBS when excited at 458 nm was acquired (Fig. 4B). It was noted that the maximum emission wavelength was located at 533 nm, which translates to the visible green luminescence of Ho^{3+} doped NaGdF$_4$ NPs. The quantum yield (QY) of the emission was also determined to be 2.4% in PBS using FITC as a reference (see Supporting Information Figure S1), which need to be further improved in vivo use.

Prior to *in vivo* imaging studies, the toxicity of TETT-NaGdF$_4$:Ho^{3+} and CTX-NaGdF$_4$:Ho^{3+} NPs against C6 and NIH 3T3 cells was assessed using an MTT assay. The obtained cell viability upon incubation with NPs at different NPs concentrations for 4 and 24 h are presented in Fig. 5. Apparently, the cells viability exceeded 90% in all

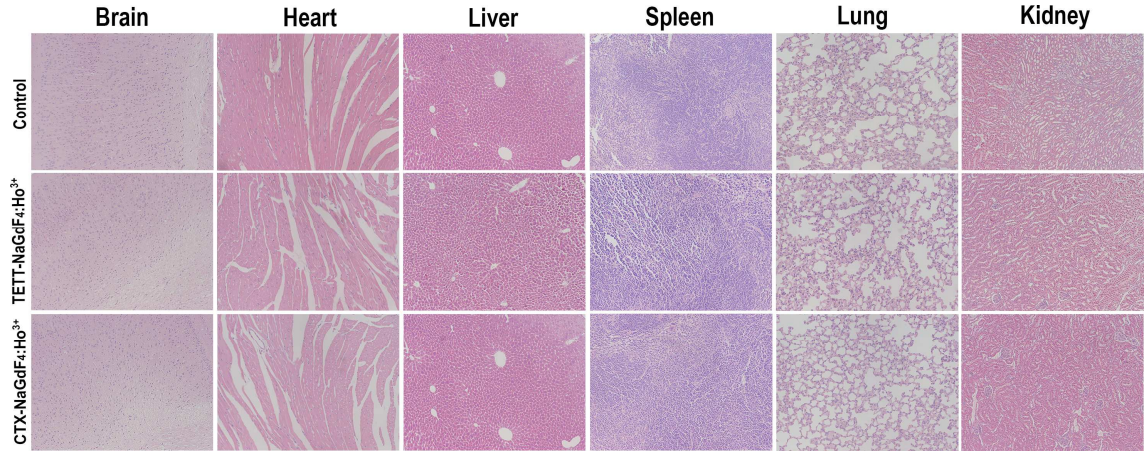

Fig. 6. H&E-stained tissue sections from ICR mice receiving no injection (control) and 15 days post-injection of TETT-$NaGdF_4$:Ho^{3+} or CTX-$NaGdF_4$:Ho^{3+} NPs (Gd concentrations = 500 μg Gd/ kg). Tissues were harvested from brain, heart, liver, spleen, lung and kidney, respectively.

investigated concentrations after 4 h incubation of NPs with or without CTX conjugation. Although prolonged incubation periods of 24 h result in a slight decrease in the cell viability, the values were still above 80% for both NPs even at a concentration as high as 360 μg/mL, demonstrating that the cytotoxicity of these nanoprobes is negligible.

Furthermore, *in vivo* toxicity of NPs was investigated by H&E staining. ICR mice were sacrificed 15 days after the administration of TETT-$NaGdF_4$:Ho^{3+} or CTX-$NaGdF_4$:Ho^{3+} NPs at a dosage of 500 μg Gd/kg and major organs were sliced and stained by hematoxylin and eosin for histological analysis. Although the dosage for H&E was higher than that used for the following MRI scan, no noticeable signs of organ damages or inflammatory lesions were observed in these major organs in comparison to control group (Fig. 6), indicating the good biocompatibility of nanoprobes.

The targeting ability of CTX-conjugated $NaGdF_4$:Ho^{3+} NPs towards C6 glioma cells was evaluated by CLSM. As shown in Fig. 7A. No obvious green fluorescence was found in C6 cells treated with TETT-$NaGdF_4$:Ho^{3+} NPs, most likely due to the insufficient uptake of NPs by C6 cells. However, upon conjugation with CTX, strong green fluorescence was clearly observed in cellular cytoplasm around the blue nuclei (stained with DAPI), suggesting an enhanced uptake of NPs by C6 cells. This was further supported by corresponding differential interference contrast (DIC) images, in which the number of CTX-$NaGdF_4$:Ho^{3+} NPs was far more than that of TETT-$NaGdF_4$:Ho^{3+} NPs in cytoplasm.

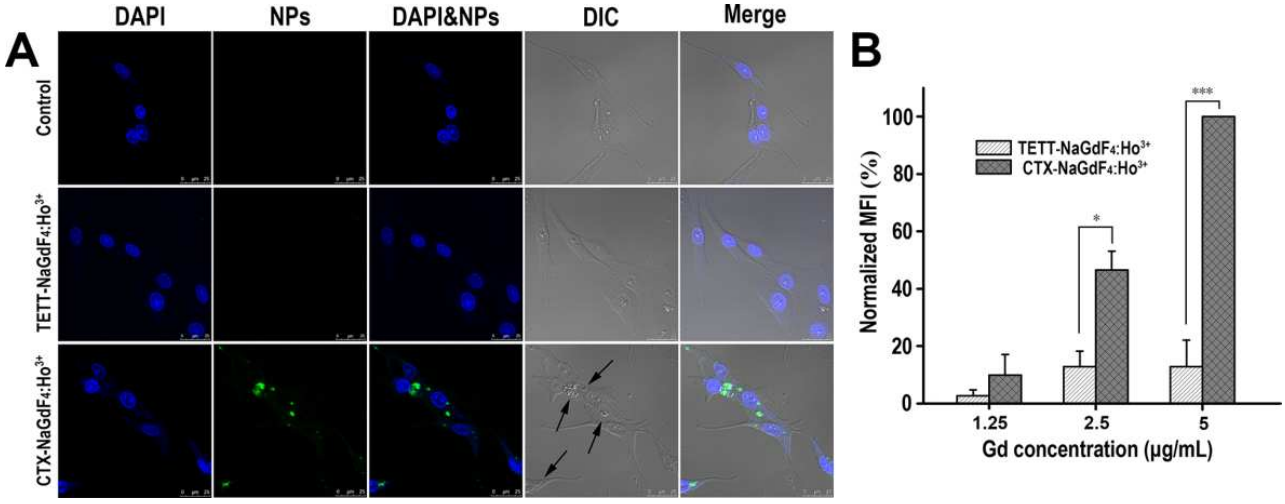

Fig. 7. (A) Confocal laser scanning microscopic images of C6 cells incubated with TETT-$NaGdF_4$:Ho^{3+} or CTX-$NaGdF_4$:Ho^{3+} NPs for 12 h at equivalent concentration of 2.5 μg Gd/mL. Cell nuclei were stained with DAPI. Green fluorescence shows the localization of NPs. Scale bar = 25 μm. **(B)** Flow cytometry quantification of C6 cells incubated with TETT-$NaGdF_4$:Ho^{3+} or CTX-$NaGdF_4$:Ho^{3+} NPs with equivalent concentrations of 1.25, 2.5, and 5 μg Gd/mL, respectively. Results represent the normalized mean fluorescence intensities (MFI) by setting 5 μg Gd/mL as 100%. (n = 3, * $p < 0.05$, *** $p < 0.001$.)

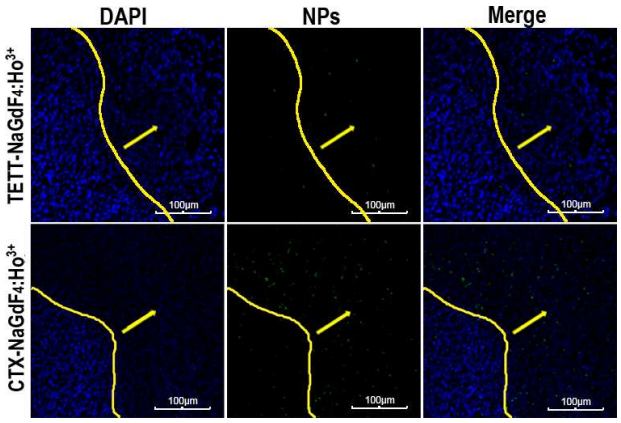

Fig. 8. Distribution of TETT-$NaGdF_4$:Ho^{3+} NPs and CTX-$NaGdF_4$:Ho^{3+} NPs in the brain of nude mice bearing intracranial C6 glioma after i.v. administration. Blue: Cell nuclei. Green: NPs. Yellow arrow points to the glioma region. Scale bar = 100 μm.

Subsequently, flow cytometry was performed to quantitatively differentiate the cellular uptake of $NaGdF_4$:Ho^{3+} NPs with or without CTX. Fig. 7B presents the flow cytometry results, in which the cellular uptakes are expressed in terms of normalized mean fluorescence intensity (MFI) by setting the MFI of 5 μg Gd/mL as 100%. Obviously, C6 cells treated with CTX-$NaGdF_4$:Ho^{3+} NPs displayed higher MFI compared to that of TETT-$NaGdF_4$:Ho^{3+} NPs at tested concentration ranges. The most significant difference in MFI was observed at 5 μg Gd /mL, which exhibited an 8-fold increase in the uptake of NPs upon conjugation of CTX. This thus verified the superior targeting ability of CTX ligands due to the specific interactions between CTX ligands and MMP-2 receptors overexpressed on the surface of glioma cells [32] which leads to an enhanced receptor-mediated internalization of NPs.

On the basis of the proved specificity of CTX-$NaGdF_4$:Ho^{3+} towards glioma cells *in vitro*, their applicability as glioma-targeted optical nanoprobes was investigated. The brain slices of C6 glioma-bearing mice treated with non-targeted or targeted nanoprobes were examined by CLSM (Fig. 8). A yellow contour line was added to visually guide the delineation of the tumor region (on the right side) from the normal tissue (on the left side). The slices treated with TETT-$NaGdF_4$:Ho^{3+} NPs exhibited sparse green fluorescent dots in both normal and tumor regions. In contrast, the slices treated with CTX-$NaGdF_4$:Ho^{3+} NPs showed great amount of green dots in the glioma region but only few green spots in the normal region, demonstrating the glioma-specific targeting ability of CTX-$NaGdF_4$:Ho^{3+}NPs. This enhanced fluorescence contrast between tumor tissue and normal tissue thus led to a clearer boundary, which might be valuable in the detection of a tiny glioma along with the delineation of the tumor margin.

Further, the feasibility of CTX-$NaGdF_4$:Ho^{3+} as glioma-specific MRI contrast agents was explored in vivo using the

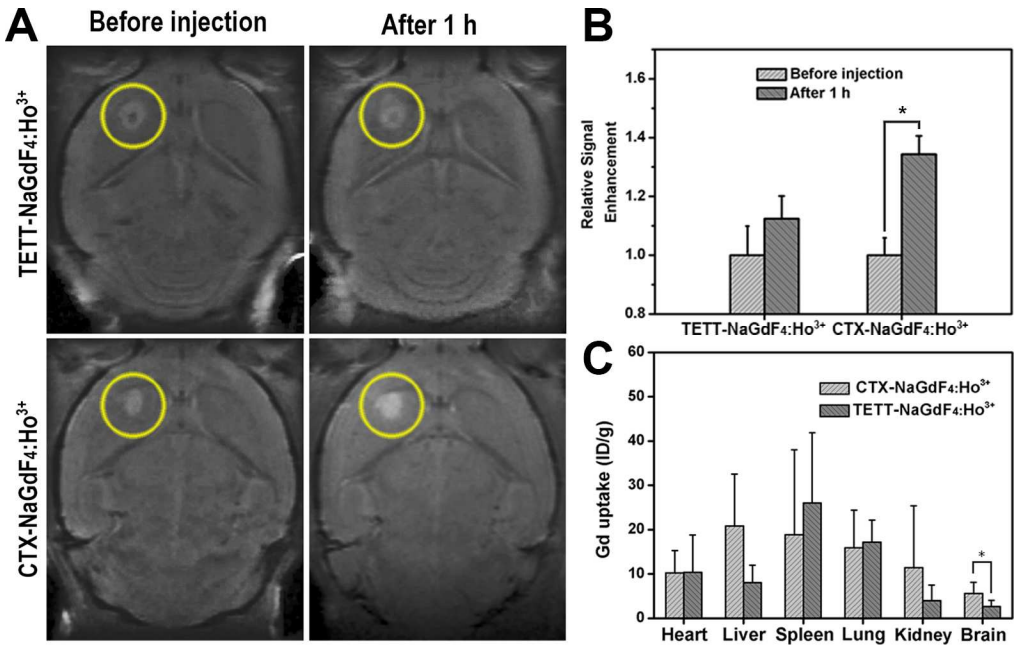

Fig. 9. (A) Two-dimensional coronal MRI images of the brain of nude mice bearing intracranial C6 glioma at pre-injection and 1 h post-injection of TETT-$NaGdF_4$:Ho^{3+} NPs and CTX-$NaGdF_4$:Ho^{3+} NPs with a dosage of 250 μg Gd/ kg. Yellow ring circles to the glioma region **(B)** Relative T_1 signal intensity in glioma (n=3, * $p < 0.05$). **(C)** Biodistribution of NPs in nude mice bearing intracranial C6 glioma, 1 h after intravenous injection (n=3, * $p < 0.05$). The Gd content in each organ was determined by ICP-AES.

tiny glioma-bearing mice on a 7 T MRI scanner. The obtained T_1-weighted MR images before and after intravenous injection of TETT-$NaGdF_4$:Ho^{3+} or CTX-$NaGdF_4$:Ho^{3+} NPs at dosage of 250 μg Gd/kg are shown in Fig. 9A. Upon injection of $NaGdF_4$:Ho^{3+} NPs, only a weak contrast enhancement was found in comparison with the pre-contrast image, indicating that the EPR effect alone would not result in a sufficient accumulation of nanoprobes in the tiny glioma. On the contrary, a significant contrast enhancement and a clearer glioma margin were observed 1 h after administration of CTX-$NaGdF_4$:Ho^{3+} NPs, demonstrating that specific targeting does improve the accumulation of NPs in the glioma region and this leads to high-quality MR images. The MRI enhancement effect was further confirmed by the quantitative analysis of MR signal intensities (SI) in the regions of interest (ROI) (Fig. 9B), which was calculated as the SI quotient for the pre- and post-contrast images (SI of normal brain tissue was deduced). It was revealed that the signal enhancement for CTX-$NaGdF_4$:Ho^{3+} NPs was about 33.3%, which was much higher than that of TETT-$NaGdF_4$:Ho^{3+} NPs (12.9%). The obvious increase in signal intensity implies that more CTX-$NaGdF_4$:Ho^{3+} NPs could be uptaken by glioma, resulting in an improved contrast.

Finally, the distribution of nanoprobes in various organs was investigated. The animals were sacrificed after intravenous administration of TETT-$NaGdF_4$:Ho^{3+} or CTX-$NaGdF_4$:Ho^{3+} NPs and brains and other major organs such as heart, liver, spleen, lung and kidney were harvested. The content of Gd in each organ (as an indicator of the distribution of NPs) was analyzed by ICP-AES. As depicted in Fig. 9C, the RES organs such as liver, spleen and lung showed higher level of uptake, while for non-RES organ such as brain, the distribution of NPs was relative low. However, a notable difference in brain distribution between non-targeted and targeted NPs was observed. The distribution of CTX-$NaGdF_4$:Ho^{3+} NPs in brain (5.57% ID/g) was about twice higher than that of TETT-$NaGdF_4$:Ho^{3+} (2.63% ID/g), demonstrating the targeting ability of CTX conjugated NPs for gliomas and this well matches the enhanced contrast effects in both MRI and optical imaging of gliomas.

Conclusions

In summary, chlorotoxin-conjugated Ho^{3+} doped $NaGdF_4$ NPs were developed as a glioma-targeted MRI/optical probe. The targeting ability of nanoprobes towards glioma cells was verified by the CLSM and flow cytometry. The *in vivo* imaging of the tiny brain glioma-bearing mice demonstrated that CTX-$NaGdF_4$:Ho^{3+} NPs significantly enhanced the contrast between glioma and normal tissue and provided a sharp boundary. In addition, the *in vitro* and *in vivo* toxicity assays proved the low cytotoxicity and the good biocompatibility of CTX-$NaGdF_4$:Ho^{3+} NPs. Therefore, our CTX-$NaGdF_4$:Ho^{3+} NPs as novel MRI/optical probes that provide complementary imaging information hold great potentials in detection of tiny brain gliomas**.**

Acknowledgments

The authors gratefully acknowledge the financial supports from the Natural Science Foundation of China (81271388, 81271639), the Scientific Research Common Program of Beijing Municipal Commission of Education (KM20110025007), the Beijing Municipal Foundation for the Talents (2011D005018000001), the Basic-clinical Key Research Grant (13JL02) from CCMU, and the Open Project Program of Key Laboratory for Neurodegenerative Diseases of the Ministry of Education (2012NZDJ01).

Notes and references

1. N. G. Rainov, A. Soling and V. Heidecke, *Neurosurgical focus*, 2006, **20**, E9.
2. R. Stupp, W. P. Mason, M. J. van den Bent, M. Weller, B. Fisher, M. J. Taphoorn, K. Belanger, A. A. Brandes, C. Marosi, U. Bogdahn, J. Curschmann, R. C. Janzer, S. K. Ludwin, T. Gorlia, A. Allgeier, D. Lacombe, J. G. Cairncross, E. Eisenhauer, R. O. Mirimanoff, R. European Organisation for, T. Treatment of Cancer Brain, G. Radiotherapy and G. National Cancer Institute of Canada Clinical Trials, *The New England journal of medicine*, 2005, **352**, 987-996.
3. A. Narayana, S. D. Kunnakkat, P. Medabalmi, J. Golfinos, E. Parker, E. Knopp, D. Zagzag, P. Eagan, D. Gruber and M. L. Gruber, *International journal of radiation oncology, biology, physics*, 2012, **82**, 77-82.
4. D. Ricard, A. Idbaih, F. Ducray, M. Lahutte, K. Hoang-Xuan and J. Y. Delattre, *Lancet*, 2012, **379**, 1984-1996.
5. D. A. Orringer, T. Chen, D. L. Huang, W. M. Armstead, B. A. Hoff, Y. E. Koo, R. F. Keep, M. A. Philbert, R. Kopelman and O. Sagher, *Neurosurgery*, 2010, **66**, 736-743.
6. E. D. Angelini, J. Delon, A. B. Bah, L. Capelle and E. Mandonnet, *Medical image analysis*, 2012, **16**, 114-126.
7. M. Watanabe, R. Tanaka and N. Takeda, *Neuroradiology*, 1992, **34**, 463-469.
8. P. Caravan, J. J. Ellison, T. J. McMurry and R. B. Lauffer, *Chemical reviews*, 1999, **99**, 2293-2352.
9. K. Luo, G. Liu, X. Zhang, W. She, B. He, Y. Nie, L. Li, Y. Wu, Z. Zhang, Q. Gong, F. Gao, B. Song, H. Ai and Z. Gu, *Macromolecular bioscience*, 2009, **9**, 1227-1236.
10. I. Miladi, G. Le Duc, D. Kryza, A. Berniard, P. Mowat, S. Roux, J. Taleb, P. Bonazza, P. Perriat, F. Lux, O. Tillement, C. Billotey and M. Janier, *J Biomater Appl*, 2013, **28**, 385-394.
11. D. Kryza, J. Taleb, M. Janier, L. Marmuse, I. Miladi, P. Bonazza, C. Louis, P. Perriat, S. Roux, O. Tillement and C. Billotey, *Bioconjugate chemistry*, 2011, **22**, 1145-1152.
12. N. J. J. Johnson, W. Oakden, G. J. Stanisz, R. S. Prosser and F. C. J. M. van Veggel, *Chem Mater*, 2011, **23**, 3714-3722.
13. F. Li, W. Gu, H. Wang, Y. Qi, Y. Deng, N. Xiao, Y. Liu, Q. Xu and L. Ye, *RSC Advances*, 2013, **3**, 5386.
14. Y. Hou, R. R. Qiao, F. Fang, X. X. Wang, C. Y. Dong, K. Liu, C. Y. Liu, Z. F. Liu, H. Lei, F. Wang and M. Y. Gao, *ACS nano*, 2013, **7**, 330-338.

15. Y. I. Park, H. M. Kim, J. H. Kim, K. C. Moon, B. Yoo, K. T. Lee, N. Lee, Y. Choi, W. Park, D. Ling, K. Na, W. K. Moon, S. H. Choi, H. S. Park, S. Y. Yoon, Y. D. Suh, S. H. Lee and T. Hyeon, *Advanced materials*, 2012, **24**, 5755-5761.
16. F. F. Li, C. G. Li, X. M. Liu, Y. Chen, T. Y. Bai, L. Wang, Z. Shi and S. H. Feng, *Chem-Eur J*, 2012, **18**, 11641-11646.
17. J. N. Liu, W. B. Bu, L. M. Pan, S. Zhang, F. Chen, L. P. Zhou, K. L. Zhao, W. J. Peng and J. L. Shi, *Biomaterials*, 2012, **33**, 7282-7290.
18. M. Weaver and D. W. Laske, *J Neuro-Oncol*, 2003, **65**, 3-13.
19. R. Huang, L. Han, J. Li, S. Liu, K. Shao, Y. Kuang, X. Hu, X. Wang, H. Lei and C. Jiang, *Biomaterials*, 2011, **32**, 5177-5186.
20. S. A. Lyons, J. O'Neal and H. Sontheimer, *Glia*, 2002, **39**, 162-173.
21. M. Veiseh, P. Gabikian, S. B. Bahrami, O. Veiseh, M. Zhang, R. C. Hackman, A. C. Ravanpay, M. R. Stroud, Y. Kusuma, S. J. Hansen, D. Kwok, N. M. Munoz, R. W. Sze, W. M. Grady, N. M. Greenberg, R. G. Ellenbogen and J. M. Olson, *Cancer research*, 2007, **67**, 6882-6888.
22. C. Sun, O. Veiseh, J. Gunn, C. Fang, S. Hansen, D. Lee, R. Sze, R. G. Ellenbogen, J. Olson and M. Zhang, *Small*, 2008, **4**, 372-379.
23. F. M. Kievit, O. Veiseh, C. Fang, N. Bhattarai, D. Lee, R. G. Ellenbogen and M. Zhang, *ACS nano*, 2010, **4**, 4587-4594.
24. J. F. Jin, Y. J. Gu, C. W. Y. Man, J. P. Cheng, Z. H. Xu, Y. Zhang, H. S. Wang, V. H. Y. Lee, S. H. Cheng and W. T. Wong, *ACS nano*, 2011, **5**, 7838-7847.
25. R. Kumar, M. Nyk, T. Y. Ohulchanskyy, C. A. Flask and P. N. Prasad, *Advanced Functional Materials*, 2009, **19**, 853-859.
26. J. Zhou, M. Yu, Y. Sun, X. Zhang, X. Zhu, Z. Wu, D. Wu and F. Li, *Biomaterials*, 2011, **32**, 1148-1156.
27. Y. Qi, C. Shao, W. Gu, F. Li, Y. Deng, H. Li and L. Ye, *Journal of Materials Chemistry B*, 2013, **1**, 1846.
28. N. Xiao, W. Gu, H. Wang, Y. Deng, X. Shi and L. Ye, *Journal of Colloid and Interface Science*, 2014, **417**, 159-165.
29. T. D. Schladt, M. I. Shukoor, K. Schneider, M. N. Tahir, F. Natalio, I. Ament, J. Becker, F. D. Jochum, S. Weber, O. Kohler, P. Theato, L. M. Schreiber, C. Sonnichsen, H. C. Schroder, W. E. Muller and W. Tremel, *Angewandte Chemie*, 2010, **49**, 3976-3980.
30. T. D. Schladt, T. Graf and W. Tremel, *Chem Mater*, 2009, **21**, 3183-3190.
31. A. López-Cruz, C. Barrera, V. L. Calero-DdelC and C. Rinaldi, *Journal of Materials Chemistry*, 2009, **19**, 6870.
32. D. Kesanakurti, C. Chetty, D. H. Dinh, M. Gujrati and J. S. Rao, *Oncogene*, 2013, **32**, 327-340.